

Iterative sparse reconstruction of spectral domain OCT signal

Xuan Liu^{1*} and Jin U. Kang²

¹*Department of Biomedical Engineering, Michigan Technological University, 403 M&M Building, Houghton, MI, 49930, USA*

²*Department of Electrical and Computer Engineering, The Johns Hopkins University Barton Hall 105, 3400 N. Charles St, Baltimore, MD, 21218, USA*

*Corresponding author: xuli@mtu.edu

Received November 30, 2013; accepted March 27, 2014; posted online April 30, 2014

We propose and study an iterative sparse reconstruction for Fourier domain optical coherence tomography (FD OCT) image by solving a constrained optimization problem that minimizes L-1 norm. Our method takes the spectral shape of the OCT light source into consideration in the iterative image reconstruction procedure that allows deconvolution of the axial point spread function from the blurred image during reconstruction rather than after reconstruction. By minimizing the L-1 norm, the axial resolution and the signal to noise ratio of image can both be enhanced. The effectiveness of our method is validated using numerical simulation and experiment.

OCIS codes: 170.4500, 100.3010.

doi: 10.3788/COL201412.051701.

Compressed sensing allows image construction from relatively few measurements^[1]. Techniques developed for compressed sensing can be powerful signal processing tools to enhance the quality of images such as ones obtained from optical coherence tomography (OCT)^[2]. In this study, we propose to use L-1 norm minimization for simultaneous OCT image reconstruction and deconvolution. One of the big technical thrusts in OCT is to improve the OCT imaging quality, including using a light source with large bandwidth and Gaussian spectral shape, optimizing reference reflectivity, using a high numeric aperture objective in sample arm, etc. Nevertheless, software approach is a cost-effective way to achieve OCT image enhancement. For example, deconvolution can improve spatial resolution of OCT image, as well as suppress side-lobes caused by the unevenness of source spectral shape. If we regard OCT as a linear shift-invariant system characterized by a point spread function (PSF) with finite spatial dimension, we can consider an OCT image as the convolution of the system PSF with the true object under imaging^[3]. In previous studies involving OCT image deconvolution, images were first reconstructed with standard OCT signal processing procedure and afterwards deconvolved with a known kernel, i.e., the system PSF, using algorithms such as Lucy-Richardson algorithm, Wiener algorithm, CLEAN algorithm, etc^[4–6]. However, the performance of these reconstruction-deconvolution approaches is highly dependent on the noise level of the raw spectral data. Moreover, these approaches would further decrease the image signal to noise ratio (SNR) after deconvolution.

In this letter, we propose and study an iterative algorithm for Fourier domain OCT (FD OCT) image reconstruction by solving an L-1 norm regularized optimization problem. L-1 norm is widely used in compressed sensing (CS) as a measure of signal sparsity^[1,2,7]. In our iterative sparse reconstruction, the spectral shape of the broadband light source of OCT system is taken into con-

sideration; therefore, our method essentially deconvolves the PSF from the blurred image during the reconstruction rather than after reconstruction. In addition, by minimizing the L-1 norm of an image, the sharpness and SNR can both be preserved. To the best of our knowledge, this approach for simultaneous reconstruction and deconvolution of OCT image has not been investigated before.

In this letter, we consider the reconstruction of individual A-scan and the PSF refers to one dimensional axial PSF.

Denoting the spatial domain object (sample) as a vector $\mathbf{x} = [x_0, x_1, x_2, \dots, x_{(N-1)}]$, Fourier domain (k-space) measurements as a vector $\mathbf{y} = [y_0, y_1, y_2, \dots, y_{(N-1)}]$, and only considering the interference term of the detected signal, we have

$$y_k = \text{Re} \left(a_0 \sum_n s_k x_n e^{-\frac{j2\pi nk}{N}} + \varepsilon_k \right), \quad (1)$$

where a_0 is a constant taking into account the system efficiency and detector response; j is the imaginary unit; x_n stands for sample field reflectivity in a small depth interval from $n\delta z$ to $(n+1)\delta z$ with the depth referenced to the zero-delay plane for reference and sample light; s_k stands for the normalized source spectral density within the small spectral interval from $k_0 + k\delta k$ to $k_0 + (k+1)\delta k$ where k_0 indicates the starting wavenumber; ε_k stands for noise term at the k th Fourier measurement bin; $n = 0, 1, 2, \dots, N-1$; $k = 0, 1, 2, \dots, N-1$. δk is the wavenumber interval between adjacent Fourier measurement bin and $\delta z = \pi/(N\delta k)$. In fact, \mathbf{x} is an OCT A-scan and \mathbf{y} is a spectral interferogram.

Equation (1) can be also written in a matrix form as

$$\mathbf{y} = \Psi \mathbf{x} + \varepsilon, \quad (2)$$

where ε is the noise vector, and Ψ is a $N \times N$ square matrix which is the product of \mathbf{S} , a diagonal matrix representing source spectral shape, and \mathbf{F} , the Fourier trans-

formation operator, as shown in

$$\psi = a_0 \mathbf{S} \mathbf{F}; S_{nk} = \begin{cases} 0; & \text{if } n \neq k \\ s_k; & \text{if } n = k \end{cases}; F_{nk} = e^{-i \frac{2\pi n k}{N}}. \quad (3)$$

In standard OCT signal processing, inverse Fourier transform (\mathbf{F}^{-1}) is applied to Fourier domain measurement \mathbf{y} . If the source has flat spectrum (s_k is identical for different values of k and we can assume $s_k \equiv 1$), \mathbf{S} is an identity matrix and thus $\mathbf{y} = a_0 \mathbf{F} \mathbf{x}$. This allows \mathbf{x} to be determined up to a scaling factor a_0 by inverse Fourier transform: $\mathbf{x} = (1/a_0)(\mathbf{F}^{-1} \mathbf{y}) = \mathbf{F}^{-1}(\mathbf{F} \mathbf{x})$. However, in a realistic OCT system, \mathbf{S} is not an identity matrix. Therefore, the result of inverse Fourier transform on \mathbf{y} is the convolution of \mathbf{x} with the system's PSF and $\mathbf{PSF} = \mathbf{F}^{-1} \mathbf{S}$, as shown in

$$\frac{1}{a_0}(\mathbf{F}^{-1} \mathbf{y}) = \mathbf{F}^{-1}(\mathbf{S} \mathbf{F} \mathbf{x}) = (\mathbf{F}^{-1} \mathbf{S}) \otimes \mathbf{x} = \mathbf{PSF} \otimes \mathbf{x}, \quad (4)$$

On the other hand, Eq. (2) shows that, theoretically \mathbf{x} can be reconstructed perfectly by multiplying \mathbf{y} with Ψ^{-1} , if the inverse of Ψ exists and $\varepsilon = 0$. However, unfortunately, Ψ is often an ill-conditioned matrix and ε is not negligible. Nevertheless, \mathbf{x} can be obtained by solving a regularized optimization problem with iterative algorithms. In this study, we use L-1 norm as a criterion for a "good" reconstruction and reconstruct \mathbf{x} by solving the optimization problem shown in

$$\begin{aligned} & \text{minimize } \|\mathbf{x}\|_1 \\ & \text{subject to } \|\psi \mathbf{x} - \mathbf{y}\|_2^2 < \sigma^2 \end{aligned} \quad (5)$$

Equation (5) poses a constrained optimization problem that can be stated in the following Lagrangian form.

$$\begin{aligned} & \arg \min_x f(\mathbf{x}) \\ & f(\mathbf{x}) = \mu \|\mathbf{x}\|_1 + \frac{1}{2} \|\psi \mathbf{x} - \mathbf{y}\|_2^2, \end{aligned} \quad (6)$$

where $\|\cdot\|_1$ indicates L-1 norm of the reconstructed image and $\|\cdot\|_2$ indicates L-2 norm: $\|\zeta\|_1 = \sum |\zeta_i|$; $\|\zeta\|_2 = (\sum |\zeta_i|^2)^{1/2}$. The first term of $f(\mathbf{x})$ quantifies image sparsity and the second term preserves data consistency; $\mu > 0$ is a constant parameter.

It is rational to solve the optimization problem that involves both L-1 norm term and data consistency term for the image reconstruction. For an image completely deconvolved from the system PSF, the data consistency term would have a small value; for an image with high SNR, L-1 norm term would have a small value. Therefore, Eq. (6) balances the trade-off between image sharpness and SNR. Various algorithms were developed to solve Eq. (6). Here we choose to use non-linear conjugate gradients (CG) and backtracking line-search algorithm. Previously, we have used this algorithm to reconstruct OCT image from randomly undersampled spectral measurements, based on the principle of compressed sensing^[2]. Details of this algorithm are shown in Fig. 1.

We first evaluated the performance of our iterative sparse reconstruction algorithm based on numerically synthesized signal. We generated a source spectrum with spectral fluctuation as shown in Fig. 2(a). According to Eq. (4), the axial PSF of the OCT system is in fact

the inverse Fourier transform of the source spectrum. As shown in Fig. 2(b), the main lobe of the axial PSF is narrow due to the large bandwidth of the source spectrum. However, the PSF has a broadened pedestal, as well as two side lobes, due to the spectral fluctuation. When A-scan is formed by convolving PSF shown in Fig. 2(a) with the depth profile of the sample, such side-lobes might introduce artifacts and lead to misinterpretation of the resultant OCT image.

Spectral domain interferometric signal is simulated assuming a mirror is placed in the sample arm at depth $z_0 = 0.5$ mm (referenced to zero-delay plane). The resultant spectral domain measurement \mathbf{y} can be obtained using Eq. (7) where $n_0 = z_0/\delta z$ and s_k takes value according to the simulated source spectrum as shown in Fig. 2(a) using

$$y_k = s_k \cos \frac{2\pi n_0 k}{N} + \varepsilon_k. \quad (7)$$

$f(\mathbf{x}) = \mu \|\mathbf{x}\|_1 + \|\Psi \mathbf{x} - \mathbf{y}\|_2^2/2$;
 $\mathbf{g} = \nabla f(\mathbf{x}) = \mu \mathbf{x}/(\mathbf{x}^* \mathbf{x} + w)^{1/2} + \Psi^*(\Psi \mathbf{x} - \mathbf{y})$ with $w > 0$
as a smoothing parameter; * as conjugate transpose of a matrix

Algorithm parameter:
 α, β : line search parameters
 M_{\max} : maximum number of iteration;
 δ -stopping criteria by gradient magnitude

Initialization:
 $m = 0; x_0 = 0; g_0 = \nabla f(x_0); \Delta x_0 = -g_0$;

Iterations:
while $((m < M_{\max}) \& \& (\|\mathbf{g}_m\|_2 > \delta))$
{
 $t = 1$;
while $(f(x_m + t \Delta x_m) > f(x_m) + \alpha t \text{teal}(g_m^* x_m)) t = \beta t$

 $\mathbf{x}_{m+1} = \mathbf{x}_m + t \Delta \mathbf{x}_m$
 $\mathbf{g}_{m+1} = \nabla f(\mathbf{x}_{m+1})$
 $\gamma = (\|\mathbf{g}_{m+1}\|_2 / \|\mathbf{g}_m\|_2)^2$
 $\Delta \mathbf{x}_{m+1} = -\mathbf{g}_{m+1} + \gamma \Delta \mathbf{x}_m$
 $m = m + 1$
}

Fig. 1. Algorithm of the iterative L-1 norm minimization image reconstruction.

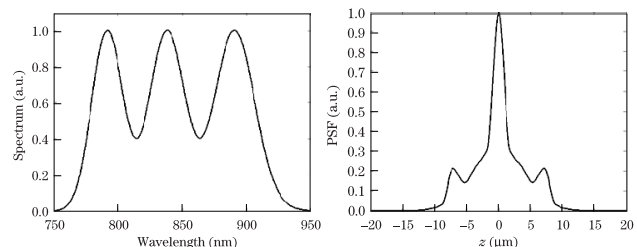


Fig. 2. (a) Simulated source spectrum and (b) axial PSF of the OCT system.

For simplicity, we let the constant a_0 to be 1 in our simulation. We also generated a random array to represent the noise term ε . An example of spectral domain signal (noise free) and additive noise are shown as red and blue curves in Figure 3(a). A spectral interferogram \mathbf{y} with noise variance $\sigma^2(\varepsilon)$ equal to 1 was simulated. Afterwards, we reconstructed A-scan by solving the optimization problem in Eq. (6) with $\mu = 1$. The result obtained from our iterative sparse reconstruction is shown in Fig. 3(b) as the red curve (linear scale). For comparison, A-scan reconstructed using inverse Fourier transform from the same simulated spectral data is shown as the black curve (linear scale) in Fig. 3(b). Both black and red curves in Fig. 3(b) are normalized to their maximum values. Clearly, the red curve has a narrow main signal lobe and significantly suppressed side-lobes compared to the black curve. To compare the SNR performance, logarithm scaled A-scans ($\mathbf{x}_{\log} = 20\log_{10}(\mathbf{x}_{\text{linear}})$) are shown in Fig. 3(c) in which the red curve has a lower noise floor. SNR of A-scan obtained from iFFT is 28 dB and SNR of A-scan obtained from our sparse reconstruction is 33 dB, indicating a 5 dB SNR enhancement.

To further evaluate the performance of the iterative sparse reconstruction, we simulated \mathbf{y} using Eq. (7) with different levels of noise variance σ^2 . A-scans were obtained from iterative sparse reconstruction, with μ equal to 0.1 and 1, respectively. We compared four parameters that quantitatively assess the reconstructed signal and showed the results in Fig. 4^[5]. The first parameter was used to quantify the image sharpness (Fig. 4(a)): $K_{\text{peak}} = (x_{i_{\text{peak}}+1} + x_{i_{\text{peak}}-1}) / (2x_{i_{\text{peak}}})$ where i_{peak} denotes the peak pixel index; the second parameter is used to quantify the effectiveness of side-lobe suppression (Fig. 4(b)): $K_{\text{side-lobe}} = (x_{i_{\text{side-l}}} + x_{i_{\text{side-r}}}) / (2x_{i_{\text{peak}}})$ where $i_{\text{side-l}}$ and $i_{\text{side-r}}$ indicate the pixel indices of left and right side-lobes. A smaller value of K_{peak} indicates a sharper signal and a smaller value of $K_{\text{side-lobe}}$ indicates a better suppression of side-lobes. In addition, we compared SNR defined as $\text{SNR} = 10\log_{10}(\mathbf{x}_{\text{max}}^2 / \sigma_x^2)$ (Fig. 4(c)) and L-1 norm (Fig. 4(d)) of the reconstructed A-scans. In Fig. 4, results obtained from iterative sparse

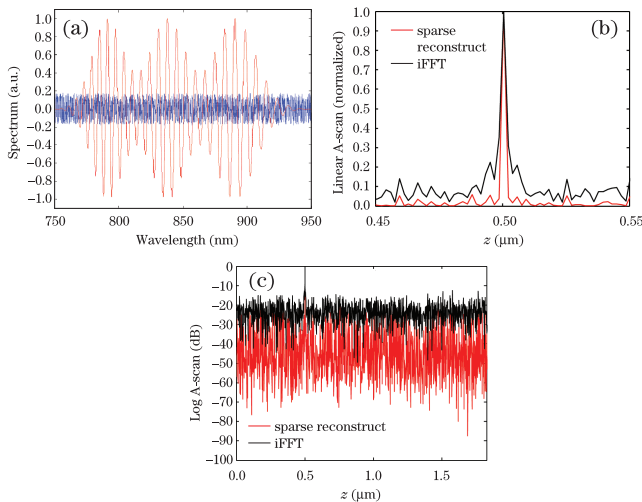


Fig. 3. (Color online) (a) Spectral domain signal (noise free, red) and noise (blue); A-scan obtained from sparse reconstruction (red) and iFFT (black) in (b) linear and (c) logarithm scale.

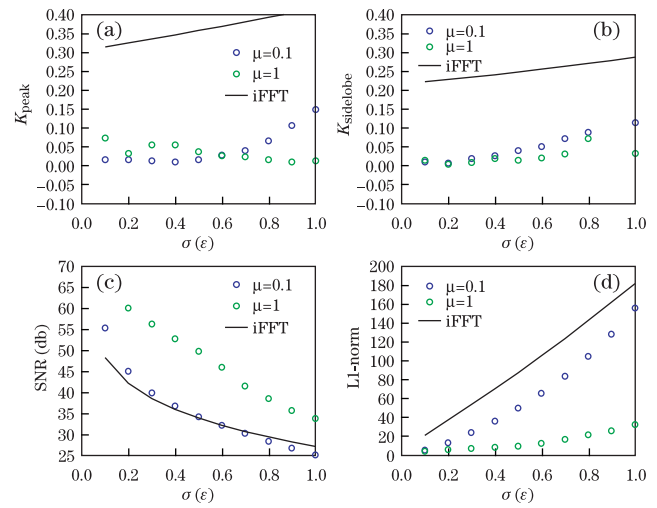


Fig. 4. Quantitate evaluation of reconstructed A-scans using different values μ under different noise levels: (a) K_{peak} that assesses peak width; (b) $K_{\text{side-lobe}}$ that assesses side-lobe suppression; (c) SNR; (d) L-1 norm.

reconstruction are shown as circles (blue circles for $\mu = 0.1$ and green circles for $\mu = 1$); while results obtained from inverse Fourier transform are shown as black curves. Figures 4 (a) and (b) show that both K_{peak} and $K_{\text{side-lobe}}$ are reduced when the proposed iterative sparse reconstruction was used. In other words, images obtained using our iterative sparse reconstruction exhibit narrower axial PSFs and significantly smaller side-lobes, at various noise levels. These imply that our method effectively deconvolves true “object” from system PSF at different noise levels. Figure 4(c) shows that our iterative sparse reconstruction algorithm improves SNR significantly when $\mu = 1$. This result is due to the L-1 norm minimization nature of the algorithm. When signal sparsity is weighed more heavily ($\mu = 1$ as oppose to $\mu = 0.1$), greater penalty is placed in pixels with small value (usually noise) compared to pixels with large values (usually signal). As a result, the large amplitude signal stays large while small amplitude signal tends to diminish; therefore a higher SNR is obtained. Figure 4(d) shows L-1 norm of reconstructed A-scans under different noise levels. Results obtained with $\mu = 1$ have smaller L-1 norm, which is as anticipated because of larger weight on L-1 norm minimization.

The effectiveness of our algorithm was further evaluated using OCT data obtained experimentally. The OCT system used is similar to the one used in Refs. [8,9]. A broadband source was used in an OCT system with a spectrum shown as Fig. 5(a). Three superluminescent diodes (SLD) were combined together coherently to serve as a light source. To achieve a large bandwidth, SLDs with large differences in central wavelengths are selected; this resulted in three peaks and two valleys in the combined spectrum and generates a PSF similar to Fig. 2(b) which has narrow main-lobe but has side-lobes with large amplitude. Using a broadband source with spectrum shown in Fig. 5(a), we obtained an OCT image of onion cells. Results obtained from our iterative sparse reconstruction and direct iFFT approach are shown in Figs. 5(b) and (c) using logarithm scale with the same dynamic range for fair comparison. Clearly, Fig. 5(b) has much

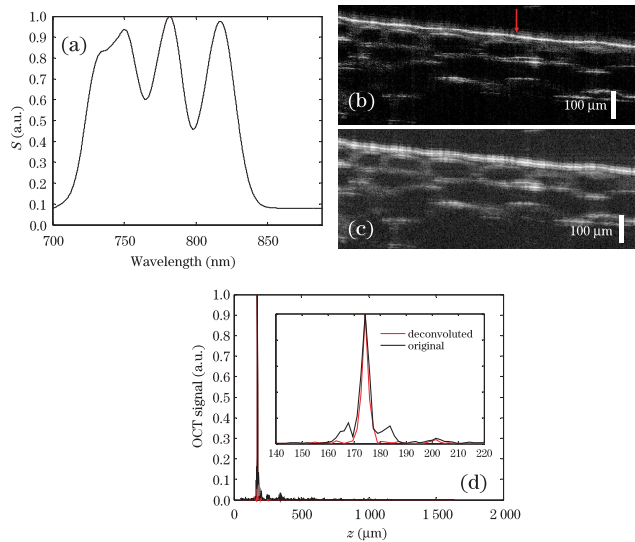


Fig. 5. (a) Spectrum of broadband source with spectral fluctuation; (b) OCT image of onion cells obtained from iterative sparse reconstruction; (c) OCT image of onion cells obtained from iFFT; (d) comparison of A-scans obtained from different approaches.

better defined cell boundaries compared to Fig. 5(c), this is because our iterative sparse reconstruction deconvolves the true image from the non-Gaussian point spread function. Moreover, L-1 norm minimization inherently reduces noise and therefore Fig. 5(b) appears to have better SNR and contrast. A-scans are selected from the same position in Figs. 5(b) and (c) (location indicated by the red arrow in Fig. 5(b)) are shown in Fig. 5(d) as red and black curves which clearly demonstrate the advantage of our iterative sparse reconstruction: suppressed side-lobe amplitude and noise level.

In conclusion, results obtained from numerical simulations and experimental OCT imaging show that the proposed iterative sparse reconstruction effectively deconvolves the axial PSF from the blurred image during reconstruction and simultaneously preserves the signal to noise ratio of an OCT image. Due to the non-

linear nature of our algorithm, when data sparsity is over-emphasized with a large value of μ , small signals might diminish to 0. However, choosing appropriate μ will allow us to reconstruct signal close to the noise floor. Our iterative reconstruction is advantageous compared to other deconvolution methods such as inverse filtering, because our method works robustly with noisy signal and preserves SNR after deconvolution. It takes 0.3 s for the computation of one A-scan using our iterative algorithm with Matlab and it takes 0.0003 s to obtain an A-scan using iFFT with the same computer. However, the iterative algorithm can be accelerated to be real-time using graphic processing unit (GPU)^[10]. The algorithm used in Ref. [10] is similar to our iterative sparse reconstruction algorithm.

This work was supported in part by the government of United States, NIH BRP grants 1R01 EB 007969 and NIH/NIE R011R01EY021540-01A1, and by internal start-up research funding from Michigan Technological University.

References

1. D.L. Donoho, *IEEE Trans. Inf. Theory* **52**, 1289 (2006).
2. X. Liu and J. U. Kang, *Opt. Express* **18**, 22010 (2010).
3. Y. Pan, R. Birngruber, J. Rosperich, and R. Engelhardt, *Appl. Opt.* **34**, 6564 (1995).
4. M. D. Kulkarni, C. W. Thomas, and J. A. Izatt, *Electron. Lett.* **33**, 1365 (1997).
5. Y. Liu, Y. Liang, G. Mu, and X. Zhu, *J. Opt. Soc. Am. A* **26**, 72 (2009).
6. M. Schmitt, *J. Biomed. Opt.* **3**, 66 (1998).
7. M. Lustig, D. Donoho, and J. M. Pauly, *Magn. Reson. Med.* **58**, 1182 (2007).
8. X. Liu, X. Li, D. Kim, I. Ilev, and J. U. Kang, *Chin. Opt. Lett.* **6**, 899 (2008).
9. J. Han and J. U. Kang, *Chin. Opt. Lett.* **9**, 090608 (2011).
10. D. Xu, Y. Huang, and J. U. Kang, *Opt. Lett.* **39**, 76 (2014).